Multiple Stages in the Aging of a Physical Polymer Gel

ARTICLE *in* MACROMOLECULES · MAY 2008

Impact Factor: 5.8 · DOI: 10.1021/ma702613j

3 AUTHORS, INCLUDING:

Yitzhak Rabin
Bar Ilan University
172 PUBLICATIONS **3,489** CITATIONS
SEE PROFILE

M. Rosenbluh
Bar Ilan University
173 PUBLICATIONS **2,686** CITATIONS
SEE PROFILE

Multiple Stages in the Aging of a Physical Polymer Gel

Nurith Schupper,* Yitzhak Rabin,* and Michael Rosenbluh

Department of Physics, Bar-Ilan University, Ramat-Gan 52900, Israel

Received November 25, 2007; Revised Manuscript Received March 3, 2008

ABSTRACT: We use multispeckle dynamic light scattering to study the dynamics of physical gelation of methylcellulose in water. Following a temperature ramp to above 55 °C, a polymer network is formed which can be destroyed upon cooling the gel. We monitor this process by detecting the total scattered light intensity which shows large hysteresis during the heating−cooling cycle. Following the temperature ramp, there is a fast initial buildup of intensity, followed by a very slow and relatively small increase. The speckle pattern does not equilibrate after very long aging times (of the order of days), even after the total scattered intensity has almost stabilized, a consequence of very slow microscopic reorganization taking place in the gel. The correlation between a speckle pattern taken at a specific aging time and subsequent patterns decays with a characteristic time that increases dramatically with the age of the gel. We find that the decay of the correlation function cannot be fitted by a single functional form in the different stages of aging; instead, four distinct stages are observed, each of which can be fitted by a different decay function. Such multiple stage relaxation is not observed in other soft condensed matter systems. On the basis of our results and those of previous studies, we argue that gelation proceeds via slow coalescence and aggregation of hydrophobic chain segments, followed by optimization of hydrophobic contacts (effective cross-links) which is opposed by network stresses due to chain stretching.

1. Introduction

A large class of soft condensed matter systems such as concentrated colloidal suspensions, emulsions, surfactant systems, micellar polycrystals, foams and pastes, display glassy dynamics.[1,2] Even below the glass transition temperature, the behavior remains ergodic for a surprisingly long time and evolves slowly depending on the time elapsed from the quench. The typical relaxation time grows with this waiting time and we say that the system ages. This phenomenon was first found experimentally in structural[3,4] and spin glasses[5,6] which display some universal scaling features, common to both kinds of glasses. The aging process[7] was described by various theoretical methods including mode coupling theory[8] and molecular simulations of Lennard-Jones glasses.[9,10] The aging dynamics of such systems is described in terms of the evolution of the correlation and response functions with the waiting time. Qualitatively speaking, these systems stiffen with age: the longer one waits, the longer is the relaxation time and the smaller the response to an external force. Physical gels in which the network is formed by temporary associations may also be out of thermodynamic equilibrium for experimentally relevant time scales. Therefore, a continuous evolution of the mechanical and dynamical properties can be observed. For example, in colloidal gels and in gels composed of multilamellar vesicles,[1,11] the correlation and response functions were indeed found to be waiting time dependent. In *physical polymer gels*, however, although such behavior has been observed,[12] it has not been investigated thoroughly. In particular, the forms of the relaxation functions, their evolution with time, and the physical mechanisms causing aging have not been studied.

In this paper, we study the aging dynamics of methylcellulose (MC), a physical polymer gel. MC is a methyl ether of cellulose, a water-soluble cellulose derivative. This polymer has numerous applications as a thickener since adding a small amount of MC increases significantly the solution viscosity. We set out to gain better understanding of the dynamics of MC gels and of their peculiar behavior as a function of temperature and the time elapsed from the formation of the gel. Since the gelation of MC is associated with changes in optical turbidity, optical methods can be used to probe its kinetics. The experimental methods used are static and dynamic light scattering (SLS and DLS, respectively). DLS is used in the scheme of multispeckle dynamic light scattering (or multispeckle photon correlation spectroscopy). Very small changes in the local configuration of the scatterers yield completely different speckle patterns and lead to a decrease in the correlation function between the respective patterns. This makes it a most sensitive and accurate method for investigating changes in local microscopic properties of random systems. Moreover, multispeckle dynamic light scattering has many advantages over the traditional method of dynamic light scattering, in that the samples can be probed both for very short and for very long time intervals, so that systems displaying nonstationary and aging dynamics can be studied.[1] By using these methods, we study scattering from gels during times of order of days and at intervals of order of seconds. This allows us to monitor both fast changes in the gel caused by intermittent events occurring during seconds and aging effects lasting for many days. In addition, we can probe whether the dynamics is smooth or sudden and abrupt, by measuring correlations between speckle patterns taken at neighboring time intervals, a method called time-resolved correlation (TRC).[13] These studies will be described in a subsequent publication.[14]

Previous studies of systems undergoing physical gelation such as in colloidal gels[15,16] and networks of multilamellar vesicles[17] found that the correlation function exhibits a two-step decay. The faster relaxation (similar to α relaxation in glasses) is described by a diffusive-like behavior yielding a stretched exponential with no age dependence. It is followed by ultraslow nondiffusive compressed exponential decay (to zero correlation), with aging-dependent relaxation time. A theoretical model was proposed which gives an expression for the rate of creation of microcollapses with aging that leads to compressed exponential relaxation.[18] The dependence of the time scales of these microcollapses on sample age was similar to that found in other systems (such as micellar polycrystals and concentrated emulsions). Other systems also showed two-step relaxation but with the second relaxation being of exponential or stretched exponential form.[11] In MC gels we also find that the correlation decreases to zero at long enough times. The intensity of scattered

* Corresponding authors. E-mail: schuppn@gmail.com (N.S.); rabin@mail.biu.ac.il (Y.R.).

10.1021/ma702613j CCC: $40.75
Published on Web 05/14/2008

light and the correlations between speckle patterns evolve with time from the moment of gel formation at constant temperature and for many hours later. Nevertheless, in contrast to other systems, it is not just the typical relaxation time that is a function of the gel's age, but the functional form of the relaxation function evolves with time during the aging process. From the variation of the relaxation function and relaxation time with aging, we identify four different regimes of relaxation and conclude that the evolution of the gel proceeds through four distinct stages.

The outline of this paper is as follows: In the next section we review the basic properties of MC gels and previous studies on these systems. In section 3 we discuss the experimental setup. Section 4 is devoted to the experimental results of the time dependence of the intensity and the relaxation of the correlation functions. In section 5 we discuss our results and present a tentative picture of the physical processes that occur during MC gelation and aging.

2. Methylcellulose Gels

MC is prepared from raw cellulose which has a degree of polymerization (DP) of the order of thousands and it has a tendency to create ordered fibrillar structures[19] stabilized by intermolecular hydrogen bonds. Due to the strength of interactions involved, cellulose does not dissolve in water and in most organic solvents. Upon substituting part of the OH groups in a glucose unit by CH_3, MC begins to lose some hydrogen bonds and cellulose layers detach from each other, thus allowing the OH groups to form hydrogen bonds with the water. There are two general classes of substitution reactions known for MC preparation: homogeneous[20–22] and heterogeneous.[23] In the homogeneous process, cellulose molecules are separated from each other in solution while in the heterogeneous process they are connected to each other by hydrogen bonds in the fibrillar structure. It is therefore assumed that in a heterogeneous reaction the distribution of the functional groups is not uniform along a single chain and from chain to chain. Commercial MC (used in this work) is a heterogeneous polymer which consists of highly substituted zones called "hydrophobic zones" and less substituted zones called "hydrophilic zones". In the homogeneous MC the substituents are uniformly distributed along the polymer chain. The degree of substitution (DS) is defined as the number of OH groups substituted in each glucose unit. The DS ranges from 0 to 3 where DS = 3 means that all OH groups are substituted. The degrees of substitution at which MC dissolves in water depend on the type of substitution: heterogeneous MC dissolves in the range of DS from 1.3 to 2.6 while homogeneous MC dissolves in water starting from DS = 0.6 to 2.0.

The most fascinating phenomenon in MC gels is their unusual property of forming gels on heating rather than upon cooling.[24] On cooling the gel, it reverts back to the sol state, that is, the sol−gel transition is reversible upon cycling the temperature. Upon gelation the viscosity increases as in usual gels and at the same time optical turbidity is observed indicating that the change in mechanical properties associated with gelation is related to creation of inhomogeneities in the system on lengths scales comparable to the wavelength of visible light. Homogeneous MC was shown not to undergo gelation[25] in the range of DS for which these samples can be solvated. Only at very high DS (>2.2) the homogeneously substituted samples showed gelation to a very weak gel as observed by ref 26.

Gelation of heterogeneous MC is assumed to take place due to association of hydrophobic regions on the polymer chains, i.e., the effective cross-links are composed of hydrophobic aggregates. The physical explanation for gelation on heating is related to the decrease in entropy in the solution state, relative to the gel. According to the mechanism proposed by Haque and Morris,[27] in the liquid state water molecules form highly constrained "cage-like" structures around the hydrophobic constituents. During gelation, as the hydrophobic segments cluster together, these cages open up, and water molecules move freely around the network. As a consequence, the number of possible configurations and the entropy of water molecules (which determines the entropy of the whole system consisting mostly of water) are low in the liquid phase and increase when hydrophobic aggregates cluster together and form a gel. The process of glass transition upon heating was demonstrated in a spin glass model (in the presence of quenched disorder),[28,29] which also explains the fact that MC is known to gel only when heterogeneously substituted, thus creating disordered or glassy states.

Many studies were conducted since the first demonstration of MC gelation,[26,27,30–39] including macroscopic measurements such as rheology, cloud point determination, gel strength, calorimetry, total amount of scattering by small-angle neutron or X-ray scattering methods, etc. Gel formation was found to be a first-order transition[40] since it is accompanied by the absorption of latent heat. In most of these studies, the elastic modulus and viscosity showed nonmonotonous behavior: below ~30 °C, they decrease upon heating but above this temperature there are two subsequent increases with temperature, reflecting two stages in the gelation process. In all cases, heating and subsequent cooling of the system showed strong hysteresis. It was concluded that the differences between heating and cooling curves stem from the fact that hydrophobic aggregation continues to take place for a long time after initial gel formation, thus leading to an increase in the measured quantity even when the temperature begins to decrease (the change of temperature rates used are fast relative to gel formation rate). The true gelation curve was assumed to be somewhere between the heating and the cooling curves. The LCST phase diagram reported in ref 41 was obtained by measurements conducted a week after formation. The two experimental techniques of cloud point determination and rheological dynamical measurements yielded somewhat different results. These loci of transitions also differ from the minimum of the elastic modulus[27] and from the phase diagram[42] derived via differential scanning calorimetry and SAXS and by visual inspection (reported only 30 min after formation). Moreover, although it was noticed in all of these studies that gelation is a time-dependent process,[43] the corresponding kinetics was not fully studied. Some authors report waiting some time before beginning their measurements, and others do not mention that the properties of these gels evolve with time. Even those who probed the aging features of the gels did not characterize them thoroughly and monitored them only up to few hours after formation.[25–27,30,31,36,37,41–43] In addition, as mentioned before, almost all measurements probed the large scale average behavior of the gel and not the internal microscopic dynamics of the system. Therefore, the phenomenon of thermal gelation of MC gels and the microscopic properties of the gel phase are not completely understood at present.

3. Experimental Details

3.1. Light Scattering Setup. The experimental setup is shown in Figure 1. Experiments are performed by scattering a frequency-doubled polarized Nd:YAG laser at a wavelength of 532 nm and power ~4.3 mW from the gel. The gel is contained inside a square glass optical cell, and the scattered light is measured approximately perpendicular to the laser propagation direction, which minimizes the effects of scattering from the gel−solvent interface. The cell is surrounded by an equilibrium bath of water contained inside a massive brass holder with three Pyrex windows: these allow incident laser light into and out of the cell, and also allow the collection of scattered light at an angle normal to the laser propagation. At this

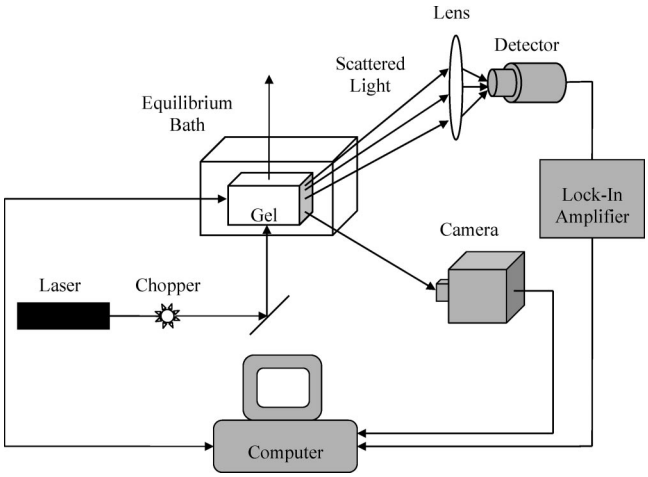

Figure 1. Experimental setup for measurement of the average intensity and speckle pattern at an angle of 90°.

scattering angle there is almost no scattering from other sources, such as windows, interfaces, etc.

The microscopic configuration of the gel is very sensitive to external parameters. Therefore, many special precautions were used in order to stabilize the system both mechanically and thermally for a long time. These will be described in what follows:

Mechanical Stabilization. The cell is mechanically isolated from its surroundings in order to eliminate vibrationally induced changes in the gel. This is done by floating the optical table upon which it stands.

Thermal Stabilization. It is found that even a change of 10 mK in the gel temperature causes some decorrelation of the scattered light patterns; the cell system is designed to allow us to maintain the temperature stable to ±0.005 °C for long periods of time. This is done as follows: a platinum resistance thermometer, PT100, is immersed in the equilibrium bath while heaters are attached to the outside of the brass container. The very small and fast response thermometer is placed inside a glass tube sealed with a metal cap so as to minimize heat conduction by the thermometer out of the cell, and it is placed as close as possible to the glass optical cell containing the gel. A Keithley model 2010 multimeter, attached to a computer, measures the temperature in the cell. Based on this measurement, a feedback loop, using a PID algorithm, is used to control the current to the heaters. The temperature could be set and maintained with high accuracy at any value between 20 and 80 °C which extends to either side of the phase transition of the gel at about 55 °C. The Keithley is set to short integration time for measurements so that the current through the thermistor during the measurement adds minimum heat to the sample. In addition, the whole equilibrium bath is enclosed by a thick thermal isolation foam. From a previous study,[44] we know that the necessary changes in temperature which cause significant changes in the speckle pattern due to thermal expansion of the materials used in the cell construction are much larger than the ±0.005 °C thermal instability in our system. Thus, simple thermal expansion does not affect the speckle patterns scattered from MC gels and the speckle pattern changes are due to the internal rearrangement of the gel network.

Pressure Stabilization. External pressure is also found to influence the microscopic gel configuration of the network (and thus the scattered speckle pattern) and therefore the gel is sealed so that at a constant temperature a constant pressure is maintained for the duration of the experiment.

Signal Stabilization. Speckle patterns can contain contributions from parasitic scattering events, e.g., scattering from the walls of the equilibrium bath. In order to eliminate interferences from walls near the scattering region, they are all colored in black. A black curtain surrounds the entire system in order to block light coming from outside. Intensity measurements (only) were performed with a lock-in amplifier in order to eliminate background noise. This is important since very small changes in the scattered intensity are measured after several days of aging.

The intensity measurements and the recording of the speckle patterns are done simultaneously. All measurements of temperature, intensity, etc. are through the Keithley and a computer program logs the sampling time and all the observed parameters.

3.2. Methylcellulose Gel Preparation. The gel is made of commercial MC (Aldrich, no. 27441-0) with degree of substitution of 1.7−1.9 and average molecular weight 88 000 g/mol. The MC is cleaned in order to get rid of all salts left from the synthesis and then dissolved in distilled water at a weight percent of 0.5%. The containers were sealed and vibrated to stir for several days. This was done very slowly in order not to create air bubbles. The gels were kept in a refrigerator at ∼5 °C for at least several days in order to obtain a uniform solution. At 0.5% concentration, the phase transition from a clear to a turbid gel is known to take place at ∼55 °C.[41] Prior to light scattering measurements, both the sample and the water in the heat bath are degassed (repeated several times) in order to eliminate air bubbles that are inevitably trapped in the process of dissolving the MC and on loading the scattering cell. The solution is very weak, i.e., it flows and moves under very small shear stresses and scatters a relatively small amount of light. After the transition to a turbid gel, the gel does not flow and it is strongly scattering. We report its scattering properties at temperatures of 57, 60, 65, and 70 °C. Higher temperatures are avoided due to problems with the evaporation of water from the scattering cell and also due to higher optical densities which result in multiple scattering. In all of our experiments the speckle patterns were found to be polarized, indicative of the predominance of single scattering events.

3.3. Experimental Procedures and Analysis. Two different measurements are performed on the scattered light: SLS and DLS. From SLS, we measure the total intensity of the scattered light, which reflects the increase in average refractive index variations as the gel forms. Due to the dependence on temperature and aging time, we measure the intensity as a function of both parameters.

From DLS we measure internal rearrangements in the gel. As mentioned in the Introduction, the multispeckle DLS has many advantages over the traditional DLS which includes extensive time averaging of the correlator output[45] in order to obtain statistically meaningful sampling. Such experiments require accumulation of data over a time scale which is several orders of magnitude longer than the time scale of the longest relaxation time of the system. For ergodic samples, time averaging directly yields the desired ensemble average. However, this is problematic for studying nonergodic samples, where time and ensemble averaging are not equivalent. Focusing the beam reduces the size of the scattering volume so that the illuminated region is not large enough to give an ensemble average. This approach is also impractical for systems where the decorrelation time is changing rapidly with the age of the sample, such that the rate of change of decorrelation does not allow one to average sufficiently. In addition, as is the case in our system, the dynamics may occur at length scales of the order of several microns, and during very long time scales (of order of days). To measure DLS under these conditions, the multispeckle DLS technique was developed. The method consists of the use of a multielement sensor, such as the pixel array of a charge coupled device (CCD) camera, to collect the signal of many speckles simultaneously.[46–49] All the pixels in the frame lie inside a small area centered on a scattering vector $\vec{q}$ and, therefore, have the same temporal statistics. The correlation functions can be calculated by averaging over all pixels. Since different speckles are statistically independent,[50] pixel averaging enhances the statistical accuracy and the total duration of an experiment can be as short as the longest relaxation time sampled. The correlation functions thus obtained are ensemble averaged, so that no special precautions are needed to investigate nonergodic samples, such as jammed systems or gels. This allows "snapshots" of the dynamics of the system to be taken, thereby directly probing the aging of the sample for many days. Nevertheless, it should be mentioned that in the opposite, short time limit, the rates of motion easily exceed what can be followed

by standard frame grabbers and the whole speckle pattern, with necessarily fewer photons per speckle spot, is more difficult to measure. Therefore, fast Brownian like motions are not monitored by our setup.

We record the speckle patterns with a CCD camera and the patterns are digitized and stored for subsequent analysis. The CCD array consists of 640 × 480 pixels, and its distance from the scattering volume is such that we record a large number of speckle spots within the camera frame in order to get good statistics. The correlation function $C_{I,\vec{q}}(t,\tau)$ is the instantaneous degree of correlation between pairs of speckle patterns recorded at times t and $t + \tau$ for a given wave vector $\vec{q}$

$$C_{I,\vec{q}}(t,\tau) \equiv \frac{\langle I_p(t)I_p(t+\tau)\rangle_p - \langle I_p(t)\rangle_p\langle I_p(t+\tau)\rangle_p}{\sqrt{\langle I_p{}^2(t)\rangle_p - \langle I_p(t)\rangle_p{}^2}\sqrt{\langle I_p{}^2(t+\tau)\rangle_p - \langle I_p(t+\tau)\rangle_p{}^2}} \quad (1)$$

where $I_p(t)$ is the intensity measured at time t for the pth CCD pixel and $\langle ... \rangle_p$ denotes an average over all pixels in the frame. Because any change in the microscopic sample configuration results in a change in the speckle pattern, $C_{I,\vec{q}}(t,\tau)$ quantifies the similarity between sample configurations at length scale $\sim 2\pi/q$ separated by time τ, at time t. From this, we can construct two one-variable correlation functions:

1. The intensity correlation function (ICF) $C_{I,t_{ag}}(\tau)$:

$$C_{I,t_{ag}}(\tau) \equiv \frac{\langle I_p(t_{ag})I_p(t_{ag}+\tau)\rangle_p - \langle I_p(t_{ag})\rangle_p\langle I_p(t_{ag}+\tau)\rangle_p}{\sqrt{\langle I_p{}^2(t_{ag})\rangle_p - \langle I_p(t_{ag})\rangle_p{}^2}\sqrt{\langle I_p{}^2(t_{ag}+\tau)\rangle_p - \langle I_p(t_{ag}+\tau)\rangle_p{}^2}} \quad (2)$$

i.e., the correlation between an image taken at an aging time, t_{ag}, and the following series of images taken with increasing time difference τ. This function gives the same physical quantity as $g_{I,\vec{q},t_{ag}}(\tau) - 1$ in traditional DLS.[51] The aging time t_{ag} is defined as the age of the initial scatterer configuration, i.e., the time elapsed from preparation of a sample at specific external conditions. The decorrelation time τ_d obtained from this analysis can then be studied as a function of the aging time t_{ag}.

2. *Time-resolved correlation* (TRC) $C_{I,\tau}(t_{ag})$.[13] By replacing variables so that τ is the fixed parameter and t_{ag} is the independent variable, we calculate the correlation between two speckle patterns recorded at a fixed time separation, τ, as a function of the aging time. The latter method allows one to discriminate between continuous and temporally heterogeneous (intermittent) dynamics. The results obtained by this analysis will be discussed elsewhere.[14]

The source of the decorrelation can be decomposed into two components, one coming from internal rearrangement of microscopic segments of the gel and the other from collective movements of large regions of the gel, a mechanical drift or slippage of the system. The latter type of motion results in an overall spatial shift of the recorded speckle pattern in a direction determined by the direction of the slippage. Such decorrelations do not represent any changes in the microscopic structure of the gel, but rather are due to the fact that the gel is contained in a glass cuvette and is relatively free to move (or due to small mechanical drifts of the glass holder). We correct for these unavoidable drifts by shifting the entire recorded speckle pattern by a few pixels in a direction which yields a maximum in the correlation function. In addition, in order to get better statistics, similar to traditional DLS, for each aging time we measure several speckle pattern pairs (at a particular aging time) and average the resulting decorrelation functions.

4. Experimental Results

4.1. Intensity during a Temperature Sweep. Upon heating the MC solution, a marked and continuous mechanical hardening of the system is observed as the physical gel is formed. In the process of gelation the almost transparent and homogeneous solution becomes turbid due to the appearance of strong inhomogeneities of polymer concentration (and, thus, of the index of refraction) and when coherent light is scattered from the gel, the total scattered intensity increases with temperature and strong speckles are observed. If the gel is subsequently cooled, the gel phase is destroyed and the MC reverts back to a clear solution which scatters a relatively small amount of light (see Figure 2 where the gel is heated from 25 to 85 °C and then immediately cooled back to 25 °C). The small residual scattering in the low-temperature phase (up to ∼50 °C) is related to the existence of small aggregates at the probed length of ∼376 nm. In this regime, both rheological studies[41] (showing an increase in G′) and DLS studies[35] (showing two decay modes for semidilute solutions, different from dilute solutions that exhibit only the first fast mode) suggest that a fragile network of aggregates is formed. This range of temperatures corresponds to the so-called "clear gel" regime in the phase diagram of reference 41. Inhomogeneities are much more pronounced upon the creation of the strong gel where the scattered intensity increases by a factor of ∼50.

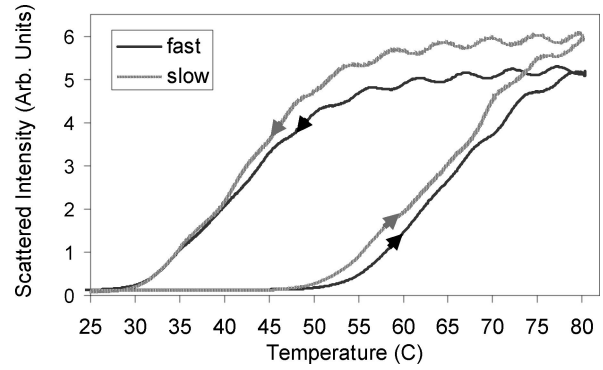

Figure 2. Total intensity of scattering upon heating and subsequent cooling of the gel of 0.5% concentration at two different rates. The fast heating and cooling rates were 1.3 deg/min and 0.66 deg/min (black curves), respectively. The slow heating and cooling rates were 0.65 and 0.33 deg/min, respectively (gray curves).

The process of gelation and melting shows strong hysteresis so that a strong gel consisting of 0.5% by weight of MC, which is formed at ∼55−60 °C, melts at ∼35−40 °C. This was observed for two heating rates of 1.3 and 0.65deg/min, and two cooling rates of 0.66 and 0.33 deg/min. Comparing these temperatures to the value of ∼50 °C obtained by cloud point measurements at 0.5% concentration after a steady state is reached,[41] we conclude that the hysteresis is associated with superheating and supercooling of the gel upon fast temperature changes. Notice that the intensity of scattered light increases with decreasing the heating rate, suggesting that the gel becomes increasingly inhomogeneous with time. The small oscillations observed in Figure 2 are an artifact due to interference effects of the light scattered from the optical windows in the cell.[44] This conclusion stems from the fact that oscillations of the same relative magnitude are observed also in the small intensity signal coming from the solution (see Figure 3). These oscillations are not in the same positions for different measurements since the temperature denoted in the figure is measured very close to the gel (in the middle of the brass holder) while the windows which are the source of the interference are at the edges of the sample holder where the temperature varies between the different heating/cooling protocols.

In Figure 2 there appears to be strong dependence of gel formation on the heating rate and rather weak dependence of final gel dissolution on the rate of cooling (∼25−35 °C). It seems that while molecular association of MC is a very slow process with strong kinetic effects, the dissolution processes are too fast to be affected by the cooling rates used. Moreover (at least from total scattered intensity measurements), the scattered intensity after cooling comes back exactly to the same

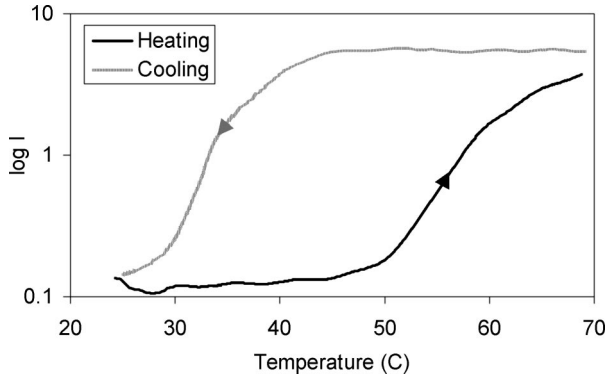

Figure 3. Total intensity of scattering upon heating and cooling (the latter after several days of aging at 70 °C). The heating and cooling rates were 1.54 and 0.7 deg/min, respectively.

value it was prior to heating. The latter effects were also observed in rheological experiments by Li[36] and by Axelos et al.[41]

These results can also be compared to those obtained by calorimetric measurements during a temperature sweep by refs 52 and 53. Upon heating a solution of concentration very similar to ours, an endothermic peak was obtained at ∼63 °C and during cooling two exothermic peaks were observed at lower temperatures: a very shallow peak at ∼42 °C and a large amplitude, wider peak at ∼34 °C. In our experiments, two subsequent decreases in the intensity are not seen, possibly because the rate of cooling is not slow enough. Indeed, in calorimetric experiments the higher temperature shallow peak was observed only at small cooling rates. Similar to the rise of the scattered intensity, the endothermic peaks depend very much on the heating rate and move to higher temperatures with increasing rate. The exothermic peaks were almost independent of the cooling rates for the rates measured, also similar to our results.

A closer view of the intensity changes can be obtained by plotting our data on a logarithmic scale as shown in Figure 3. Inspection of this figure suggests that the formation of the gel occurs in two stages: an initial small increase in light scattering in the range 30−50 °C as the "soft gel" phase is formed, followed by steep rise associated with the formation of the "strong gel", from ∼50 °C and on. In the "soft gel" regime, a tenuous network is formed which scatters light only slightly more strongly than the solution. The "strong gel" is the high turbidity state that corresponds to a strong network with large-scale polymer concentration inhomogeneities.

Notice that for the measurements reported in Figure 3 the sample was heated up to 70 °C and kept at this temperature for several days before the cooling process began. The intensity difference between the end of the heating curve and the beginning of the cooling curve is due to this "aging" and can be attributed to the continuing process of network formation and coarsening during the aging period at 70 °C. In addition, the beginning of the gel dissolution in this case occurs only once a sufficiently low temperature is reached; there is no decrease in the scattered intensity down to ∼45 °C, in contrast to the data shown in Figure 3. The reason for the difference is that the more heavily cross-linked network formed during the long time the gel was maintained at high temperature is more stable than that formed when the gel was cooled immediately upon reaching 70 °C. Only when the temperature is low enough does the network break up, resulting in an abrupt decrease of the scattered intensity.

4.2. Stabilization at a Constant Temperature. *4.2.1. Intensity Measurements.* After heating the solution to a fixed temperature above the gel point, the total intensity of scattered

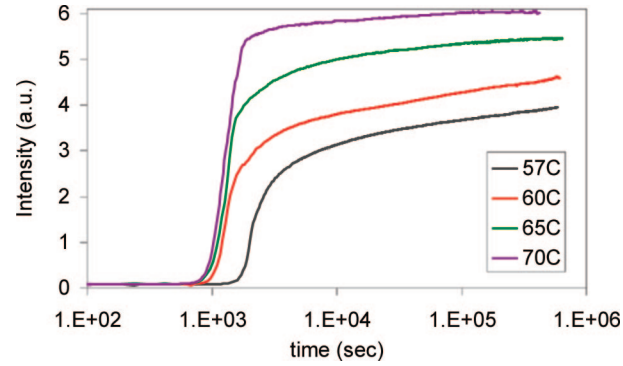

Figure 4. Total intensity of scattered light from a gel of 0.5% concentration at an angle of 90° and constant temperatures of 57, 60, 65, and 70 °C (±0.005) versus time. The data is plotted on a semilogarithmic scale from the time of initialization of the temperature ramp and up to several days later. All samples initiated at 25 °C and were temperature ramped to the desired temperature, a process which took around 15 min. Gel formation begins somewhat before this time and is faster for the higher temperatures. The increase in the intensity appears to contain two different timescales: a very short formation time of order of minutes to a few hours and long stabilization of order of days.

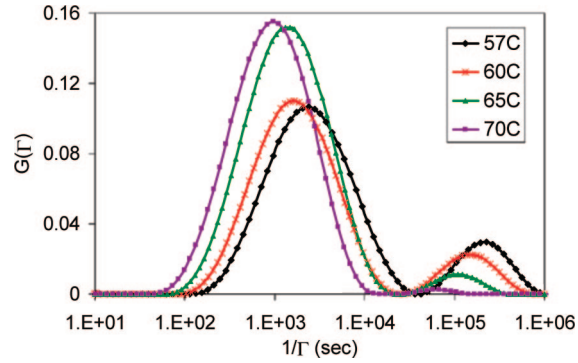

Figure 5. Decomposition of the intensity rise signal from Figure 4 into temporal components by inverse Laplace Transform routine for the four different temperatures measured. The results show two processes occurring on two different timescales in the system: a short and strong component and a long and relatively weak one. As the temperature rises the time scales for both processes become shorter and the contribution of the faster processes to the overall intensity becomes larger.

light continues to increase for a very long time. Figure 4 shows the intensity as a function of time plotted on a semilogarithmic scale for the four temperatures measured. The data is plotted from a short time after initialization of the temperature ramp and up to several days later. All samples were initiated at 25 °C, and then temperature was ramped to the desired temperature, a process which took around 15 min from the beginning of gel formation. At higher temperatures, higher intensities are reached and stabilization occurs at a faster rate. Thus, while for the highest temperature reached in our study, 70 °C, the intensity seems to reach a constant value during the time of the experiment, at lower temperatures intensity continues to rise significantly even after a week of measurements.

The intensity increase vs time shows the existence of relaxation processes with multiple time scales in the system. In order to determine these time scales and their relative contribution to the overall increase in the intensity we decompose the data into their temporal components using the inverse Laplace transform routine CONTIN.[54] The routine converts measured signals into distributions of rates $G(\Gamma)$, as shown in Figure 5 for the four temperatures. In order to obtain the timescales of stabilization at a constant temperature, the intensity data up to

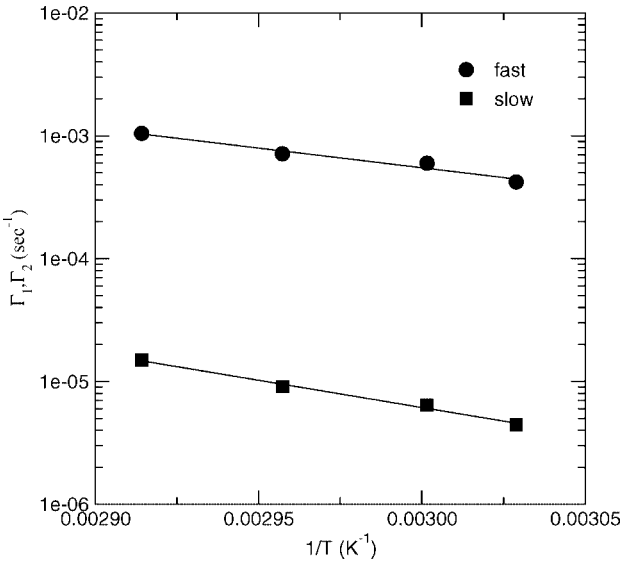

Figure 6. Logarithms of short and long decay rates in the system as a function of inverse temperatures. The activation energies of $\Delta E_1 \sim (22.2 \pm 3.1)kT$ and $\Delta E_2 \sim (30.6 \pm 1.9)kT$ at 60 °C are obtained from the exponential fit (straight solid line).

Table 1. Maximal Values of $G(\Gamma)$ of Figure 5 at the Four Temperatures Measured

T (°C)	$\tau_1 = 1/\Gamma_1$ (s)	$\tau_2 = 1/\Gamma_2$ (s)
57	2380	225000
60	1670	156000
65	1400	110000
70	960	66900

~8 min after initiation (approximately the time at which the strong gel is formed, as reflected by the steep rise in scattered intensity) was truncated before applying the analysis by CONTIN. The error related to the exact position of the signal truncation is relatively small for time scales beginning from ~500 s.

For each temperature, as seen in Figure 5, stabilization proceeds in two stages: a fast and considerable initial growth of the scattered intensity of the order of minutes to hours followed by a very slow and relatively small increase, i.e., long stabilization of order of days. The distribution of the initial rise times is peaked at about a value τ_1, of the order of several hundreds to thousands of seconds, and that of the long rise times is centered about τ_2, of the order of hundreds of thousands of seconds i.e., days (see Table 1). Both of these times decrease pronouncedly with temperature and the relative contribution of the short time processes is larger at higher temperatures. From the larger area under the first portion of the plot of $G(\Gamma)$, we deduce that most processes of inhomogeneity formation in the system end in the first stage. The remaining increase in scattered intensity occurs during a second (much longer) stage and is attributed to coarsening resulting from slow rearrangements of the reversible cross-links in the system. This accounts for the shortening of time scales as the temperature increases, since when the temperature is higher the driving forces for segregation (i.e., the hydrophobic interaction) increase and the relevant times are shorter.

The different time scales of the system are the result of different activation energies of the various aggregation processes. Therefore, we can fit the temperature dependence of both the fast and the slow processes in an Arrhenius plot in order to estimate the activation energies involved. From the fitting shown in Figure 6, we obtain the following activation energies at 60 °C: $\Delta E_1 \sim (10.2 \pm 1.4) \times 10^{-20}J$, $\Delta E_2 \sim (14.1 \pm 0.9) \times 10^{-20}J$, i.e. $\Delta E_1 \sim (22.2 \pm 3.1)kT$ and $\Delta E_2 \sim (30.6 \pm 1.9)kT$. Therefore,

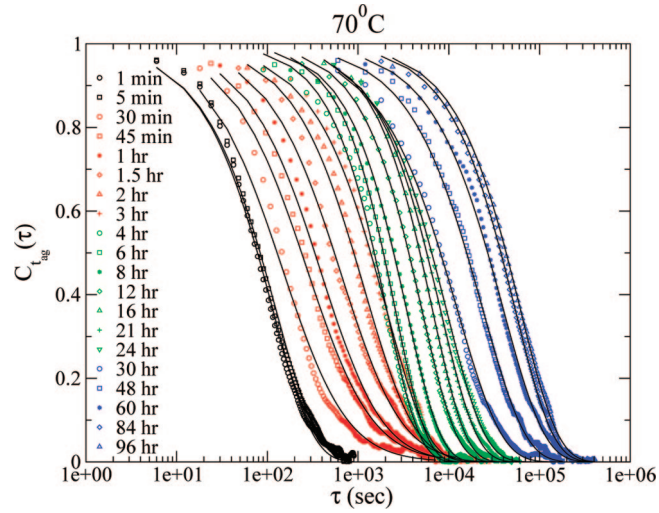

Figure 7. Correlation function of speckle patterns measured by multispeckle DLS at 532 nm and a scattering angle of 90°, for a sample of 0.5% concentration at 70 °C. The results are shown for different aging times t_{ag} after gel formation. Lines are exponential (stretched for black and blue data and compressed for green data) and power law (for red data) fits.

we conclude that during the initial process of network formation by aggregation of hydrophobic chain segments, the activation energies involved are relatively small. However, when the system is already partially cross-linked, activation energies for further rearrangements increase and the corresponding time scales become longer.

The observed increase of the scattered intensity with time at constant temperature is a crude measure of the overall change in the state of aggregation of the gel. In order to directly probe the processes occurring in the system, we use multispeckle DLS which monitors the variation in the speckle patterns. A change in the position of the scatterers on length scales of the order of a fraction of the wavelength of the probing light will cause complete decorrelation in the scattering picture, and yet may cause no change in the total scattered intensity. Even at very long times, when no significant intensity changes can be detected, the scattered speckle pattern still varies with time and provides information about the continuing microscopic rearrangement processes occurring in the gel.

4.2.2. Intensity Correlation Function. We record the speckle patterns as the gel evolves and ages from the start of a temperature ramp and up to more then 7 days after formation, at a constant temperature. We calculate the correlation (eq 2) between a speckle pattern recorded at a specific aging time t_{ag} and a subsequent speckle pattern recorded at a variable time delay, τ.

For the three higher temperatures (60 °C and up), gelation begins already during the temperature ramp, even before the set point temperature is reached; we define $t_{ag} = 0$ as the time when the set point temperature is attained to within the experimental accuracy ($\pm 0.005°C$). However, at lower temperatures (57 °C) gelation is slower than heating and there is some ambiguity in defining the zero of the aging time. Therefore, for lower temperatures, we define $t_{ag} = 0$ to be the gelation time as detected by the sudden slowing down of the very fast motions of the speckles as the gel is formed. The uncertainty in determining t_{ag} is of the order of tens of seconds, which is small compared with typical values of t_{ag} that can be as long as several days.

Figure 7 shows typical intensity correlation functions at a fixed temperature of 70 °C for various initial ages of the sample, on a semilogarithmic scale. Only a limited set of representative

intensity correlation functions are shown (to avoid overcrowding of data points), but the decorrelation functions of more aging times were measured and used in the following analysis. For all aging times the correlation function exhibits a gradual decay to zero (or to a small value due to very long decorrelation processes which are difficult to follow since the value of the correlation is small). The decay of correlations for very short aging times, of the order of seconds, is extremely fast, of the order of 0.1 s, and is not shown in the figure. The complete loss of correlation indicates that rearrangement processes occur on the length scale of the probing wavelength.

From Figure 7 it is evident that, even after very long aging times, the microscopic configuration of the gel does not stabilize and the correlation decays with typical aging-dependent relaxation dynamics. Thus, despite the solidlike rheological behavior of the gel and the observation that the total scattered light intensity has nearly stabilized (indicating that the average index of refraction inhomogeneity approaches a constant value), the correlation continues to decay, and we conclude that the local reorganization of the gel continues even for the longest observation times. At 70 °C the dynamics slows down with sample age by approximately 2 orders of magnitude in the first day of aging; for aging time of 1 min the decorrelation time is 114 s (∼2 min), while upon aging for 1 day the decorrelation time becomes 9300 s (∼2.6 h). The decorrelation time continues to increase during the following 3 days and reaches 61 100 s (∼17 h) after 96 h (Figure 7). The observation that the decorrelation time τ_d increases dramatically with aging time t_{ag}, appears to suggest that either equilibrium or a glassy state with frozen-in dynamics will be eventually attained. However, if such a state exists, the time to reach it is very long and it could not be observed in our current experiment.

Similar results are obtained at other temperatures, and those of 60 and 57 °C are shown in Figure 8, a and b, respectively. In general, at lower temperatures, the decorrelation times become longer (for the same aging times), and the speckle patterns become more stable. This is different from the usual glassy behavior, where the deeper the quench, the slower the evolution. Here, the transition is of "inverse freezing" type,[28,29] and the larger the temperature ramp is, the faster are the kinetics. In fact, this type of kinetics is characteristic of normal phase separation (in ergodic systems), in which the driving force for segregation increases with quench depth and the processes become faster.

More careful examination of Figures 7 and 8 reveals that, at all temperatures, the correlation functions change their form during the experiment and four distinct regimes of relaxation can be identified (for clarity each regime is colored differently in the figures). While, in the first stage, the correlation function decays rapidly to zero, in the second stage the decay becomes more moderate and a long tail appears. In the third stage, the correlation function becomes progressively steeper and falls abruptly to zero with a relatively short tail. In the fourth regime, the relaxation function broadens again and the form of the tail becomes similar to that observed in the first regime. The above partitioning is somewhat arbitrary as there are no sharp transitions from one regime to the other. It is important to note that at all stages (even those exhibiting relatively short tails) the relaxation times gradually increase with aging. It is the *rate of change* of the relaxation times which changes between stages thus altering their forms.

Comparing the data in Figure 7 and 8, one observes that at higher temperatures the system passes through the above-mentioned stages faster than at lower temperatures. Thus, while region 1 is observed only for ∼20 min at 70 °C and region 4 is reached after 1 day, at 57 °C region 1 lasts for ∼8.5 h and region 4 is reached only after ∼4 days (at the longest aging

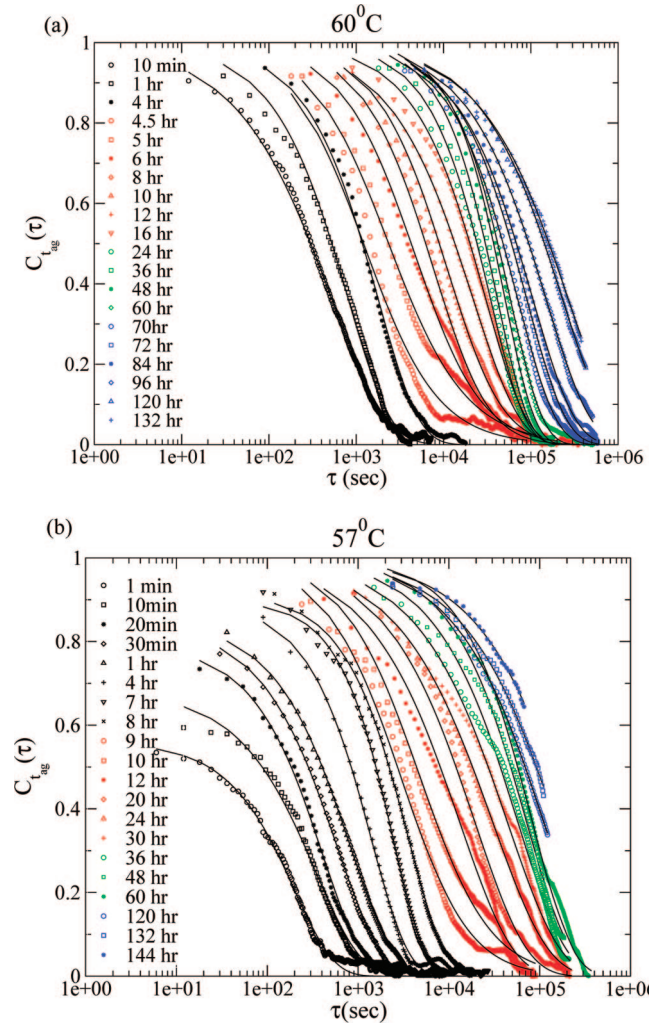

Figure 8. Same as Figure 7 but at (a) 60 °C and (b) 57 °C. The results are shown for different aging times t_{ag} after gel formation. Lines are exponential (stretched for black and blue data and compressed for green data) and power law (for red data) fits. Note that for short aging times (especially at 57 °C), the correlation does not appear to start from 1 in the limit of vanishing delay time (indicative of the presence of a very fast unobserved relaxation process).

times the curves are truncated in some of the figures since the experiment ended before the decorrelation was complete). From this, we conclude again that as the temperature increases, the driving forces for gelation increase too, and the gel evolves faster. As discussed in the previous section, this was manifested by increasing scattered intensity and decreasing time to reach steady state, with increasing temperature.

In order to study this behavior more quantitatively, we fitted the curves with two different functional forms. From the fitting we can extract the characteristic decorrelation time, $\tau_d(t_{ag})$. In regions 1, 3, and 4 we find that the curves can be fitted by exponential functions of the form (shown by the solid curves in the figures)

$$C_{t_{ag}}(\tau) = \exp\left[-\frac{\tau}{\tau_d(t_{ag})}\right]^{\alpha(t_{ag})} \quad (3)$$

Such exponential forms are often used to describe the slow relaxation processes encountered in many glassy systems.[1–3,11] At 57 °C in region 1, the fitting formula consisted of another multiplicative parameter to the stretched exponential function whose values increase with aging time from 0.56 at 1 min to 0.915 at 8 h. At higher aging times this parameter is not required.

The introduction of this parameter is necessary since as can be seen in Figure 8b the measured relaxation starts at values lower than 1. Its physical meaning will be discussed below. From the fits we conclude that despite the marked differences in the characteristic decorrelation times, the correlation functions measured at different stages can be fitted by introducing an aging-dependent stretching exponent α. In regions 1 and 4 the best fit corresponds to a stretched exponent, $\alpha < 1$, while in region 3 the exponent is compressed, $\alpha > 1$.

In region 2 the correlation function has a very long tail and a power law is more appropriate to describe the decay

$$C_{t_{ag}}(\tau) = \left[1 + \frac{\tau}{\tau_d(t_{ag})}\right]^{\beta(t_{ag})} \quad (4)$$

Such power law decay was observed in many gels and other systems.[1,55−58] However, while in MC gels the correlation always decays to zero, in other systems a power law decay to a finite background is observed in the nonergodic (gel) state and stretched exponential relaxation occurs in the sol, when approaching the glass (or the gel) transition. This stretched exponential form is characteristic of a broad distribution of relaxation times as a result of a broad distribution of cluster sizes. When the system becomes nonergodic, the correlation changes from stretched exponential to power law as infinite relaxation times appear in the system and the stretched exponent approaches $\alpha = 0$. Here, we conclude that the power law behavior (in region 2) is the result of the appearance of very long relaxation times in the system (relative to the highest contributing modes of this relaxation). Note that although the quality of the fit is not so good at the beginning of the second stage, it improves with aging time. The reason for this is related to the tremendous lengthening of the relaxation times at the beginning of this stage which makes the tail of the correlation function much longer then the initial (almost) exponential decay.

Compressed exponential relaxation which was found to be the most appropriate functional form to fit stage 3, is similar to late-stage relaxation in colloidal gels, concentrated emulsions and concentrated surfactant phases.[11] In these systems, the correlation function first decays exponentially (with a simple exponent) to a plateau and then decays to zero with a compressed exponential form. This second decay is similar to what we observe in stage 3 but with somewhat larger exponents, between 1.3 and 1.5[1,59] (we obtain ∼1.1−1.25, see Figure 11). This dynamics was attributed to the buildup of internal stresses in the system as the jamming transition is approached and the mobility vanishes.[18] In any case, such relaxation is an indication of fast processes (relative to the typical time scale) that occur in the system.

We would like to comment on the two-step relaxation found in all of the above-mentioned experiments where there is a fast initial decay in the correlation (of the order of milliseconds) before the final, slow decorrelation stage. This first decorrelation is ascribed to thermally activated diffusive motion of the scatterers, due to its exponential form and q^2 dependence. In our experiments we observe only the long decorrelation times, presumably because the time scales of the initial decorrelation are too fast to be captured by the frame capture electronics (as the patterns are recorded at intervals of 6 s). In order to study the fast process, one has to use traditional DLS methods, i.e., apparatus working at millisecond time scales. However, from visual inspection of a fast changing background in the speckle patterns, it is clear that such fast initial decay of the correlation is always present. This fast relaxation is the reason that the data at the first stage at 57 °C begins at values lower than 1. As mentioned earlier, at 57 °C gelation is much slower than at higher temperatures and therefore, even after the gel is formed, there is still a significant presence of liquidlike regions (sol

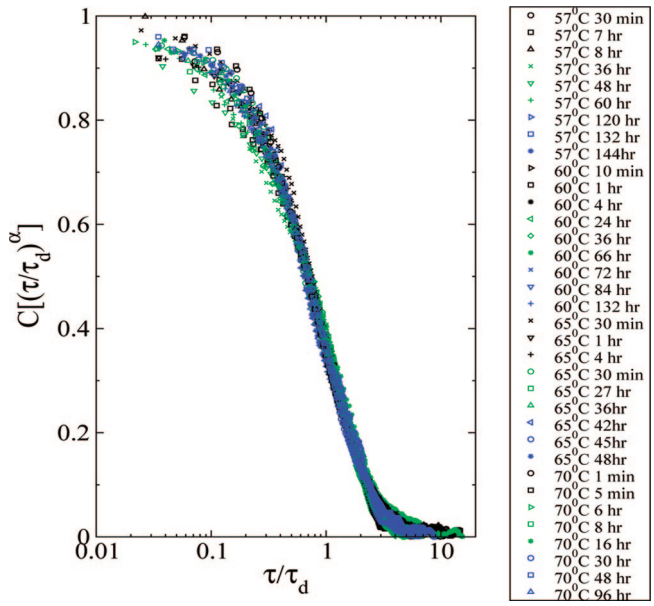

Figure 9. Scaling of the autocorrelation functions calculated at different aging times and different temperatures of the gel. Representative curves from regions 1, 3, and 4 are plotted. The values used for the fit of τ_d and α are those shown in Figures 10 and 11, respectively.

fraction) in the system. These regions contribute to the scattered intensity, and their fast dynamics leads to relaxation on time scales that are too short to be observed by our experimental method. As gelation proceeds, the liquidlike contribution decreases and the correlation functions start at a value of almost 1, as expected.

Further evidence for the existence of a liquidlike component in the system is provided by measurements of the correlation between each two subsequent pictures taken with a time lag of 6 s (TRC analysis[14]). The average of the TRCs with time over aging times in the fourth stage where the decorrelation times are very long are ∼0.92 at 57 °C, ∼0.97 at 60 °C, and ∼0.98 at 70 °C. These are much lower than expected (>0.992) for such a short time lag during these large aging times. Furthermore, the TRC between two pictures taken at a fixed short time difference should remain higher for a longer time at low temperature than at higher temperatures; the opposite temperature dependence is observed. The stability of our system was checked and it was found that the correlation function between speckle patterns scattered from a glass sample maintained at a constant temperature, is stable at a value of ∼0.995 for many hours.[44] Therefore, the relatively low average values of the TRC are not due to apparatus limitations but result from a real, very fast relaxation in the gel. We conclude that there is a small liquidlike component in the gel, with typical decorrelation time much less than 1 s, which reduces the correlation between two consecutive speckle patterns. This accounts for the fact that the average of the TRC data is lower at lower temperatures, since the contribution of the liquidlike constituent to the speckle patterns is higher at those temperatures.

Instead of using the actual measured times in plotting the correlation functions, we can use a scaled time to plot the correlation as a function of $[\tau/\tau_d(t_{ag})]^{\alpha(t_{ag})}$ and attempt to collapse the correlation functions for different aging times and different temperatures onto a single master curve. We plot only the curves for regions 1, 3, and 4 which are all well fitted by exponentials and these converge to the master curve shown in Figure 9. This illustrates again the changing behavior of the system during its aging as the stretching of the exponent changes between stages.

Qualitatively similar master curves have been obtained for different soft disordered systems. However, the specific behavior

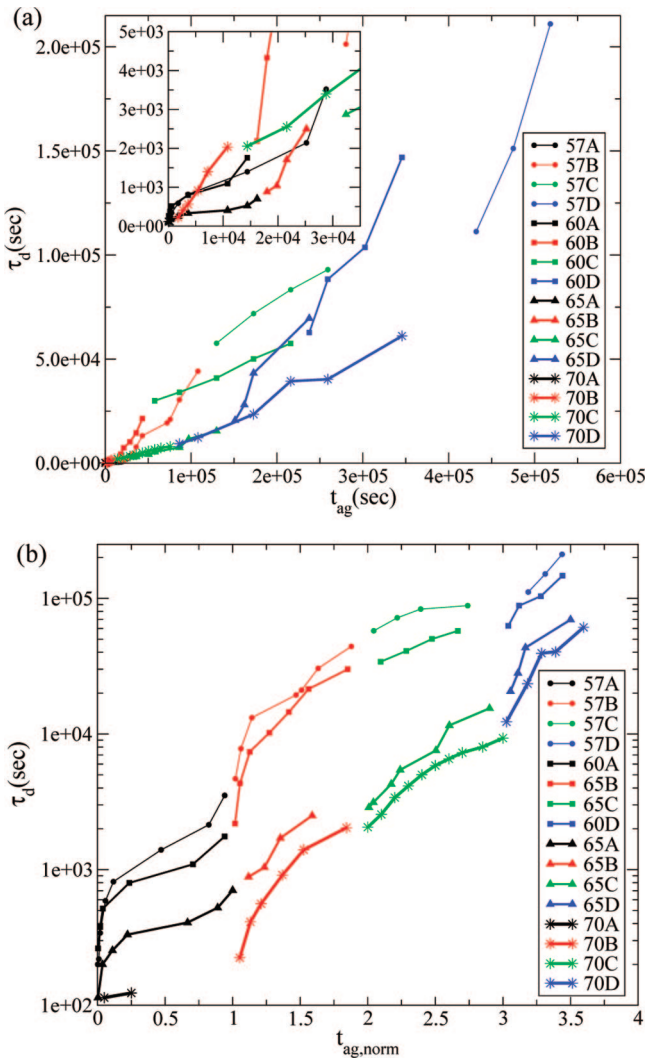

Figure 10. (a) Aging time dependence of the characteristic decorrelation times for the different temperatures. Different temperatures are denoted by different symbols and line widths, and the four stages (labeled as A, B, C, and D) are colored as previously. The inset shows an expanded view of the initial stage at the four temperatures. During the four stages of aging, the rate of the increase changes: in the first stage there is a moderate increase, in the second it is steeper, during the third it is again lower, and in the fourth stage the increase is higher once more. (b) The same data shown on a normalized time scale where the *x* axis is the effective age of the sample on a scale from 0 to 4 as defined in the text. With this calibration the data shows clear decrease of decorrelation times with temperature.

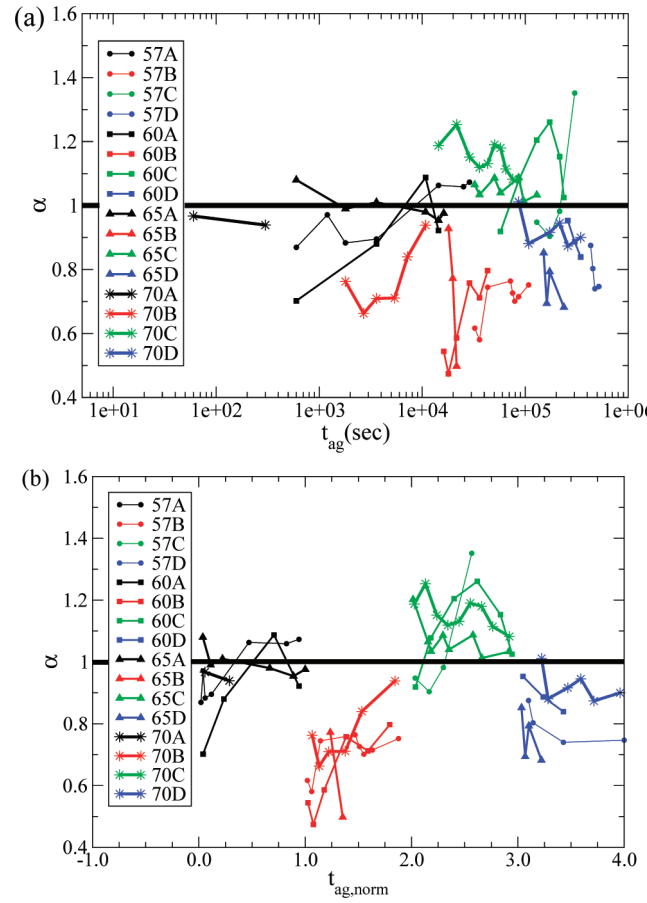

Figure 11. (a) Stretching exponent α of the correlation function as a function of the aging time (plotted on a logarithmic scale) for a gel at all four temperatures. Different temperatures are denoted by different symbols and line widths, and the four stages (labeled as A, B, C, and D) are colored as previously. (b) The same data shown on a normalized time scale where the *x* axis is the effective age of the sample on a scale from 0 to 4 as defined in the text. In all cases, the stretching exponent shows an initial value close to ∼1 (stage 1), followed by a decrease to much lower values (stage 2), then increases again from the minimum approaches 1 and jumps to above 1 (stage 3). Finally, it decreases back again to below 1 (stage 4).

of multiple stage relaxation processes upon aging has not been observed until now. Usually, the stretching exponent is either a constant[1] or decreases with the sample age.[60] A constant stretching exponent indicates that the width of the distribution of relaxation times in the system relative to the main contributing mode does not change during the aging of the sample. A decreasing exponent indicates that the distribution of relaxation times becomes broader as the system ages. In our case, the width of the distribution of relaxation times relative to the central mode displays a complex behavior during the aging of the gel. At first, the width decreases mildly (increasing the stretching exponent), then it increases significantly (the stretched exponential changes into a power law); in the third stage it decreases appreciably (during the transition to a compressed exponential), and finally it increases again (transition to a stretched exponential behavior).

Further evidence for the existence of four stages in the evolution of the gel comes from the dependence of the decorrelation time τ_d on the sample age t_{ag} (Figure 10a). At all temperatures, the decorrelation time gets longer with sample age; however, the rate of increase varies between the different stages. Since there are not enough data points to determine the functional dependence of the increase with aging time, we will only consider the average slope at each stage. During the first stage of aging, the average slope is relatively small and it increases abruptly during the second stage. The third stage (transition to a compressed exponential form) again shows a smaller average slope and, in the final stage, the average slope increases sharply again. Such a behavior differs from the linear dependence on aging time found in many glassy systems[61] which is referred to as "simple aging". In other aging soft matter materials, the decorrelation time was found to increase at a rate slower than linear with aging time,[15,17,62] though higher than linear dependence was also found.[13,63,64] A nonmonotonic behavior with sample age, however, was not reported before.

Although the time scales are usually longer at the lower temperatures, this is not always the case, as can be seen from Figure 10a. For example, after 12 h (43 200 s) the decorrelation for the 60 °C sample takes longer than at 57 °C. This observation is consistent with the expectation that the kinetics of aging depends on the temperature and that, at two different temperatures, the gels may be in two different stages of aging. For

example, the 60 °C gel is already at the end of stage 2 after the sharp increase in time scales, while for 57 °C the gel is still at the middle of stage 2 where decorrelation times are shorter. Since the decorrelation time for a given stage gets shorter as the temperature increases, we can define an effective age of the system which is a function of both temperature and aging time. The effective aging time $t_{ag,eff}$ is a number between 0 and 4 and gives the state of the system at a specific aging time. We define it by $t_{ag,eff} = (t_{ag} - t_{n-1})/\Delta t_n + (n - 1)$, where t_n is the end time of stage n, and Δt_n is its duration. Since there is a small gap between the aging times for which the correlation functions were calculated, the end time of a stage is taken as the middle time between the last aging time corresponding to this stage and the first aging time of the subsequent stage. Also, since the end of stage 4 is not reached in our experiments, we have to extrapolate it from previous stages and it is taken to be 5 times longer than the third stage (for the corresponding temperature). The results of this transformation are shown in Figure 10b: at the same effective age, at higher temperatures the system has a shorter decorrelation time than at lower temperatures.

In the total scattered intensity analysis described in the previous section, it was found that there are two time regimes, an initial sharp increase in scattered intensity, followed by a much more gradual increase. We find a correspondence between these time scales and the time scales of the different stages in the decay of the speckle correlation. The sharp initial rise in the intensity is found to occur during the first stage of the aging process while the subsequent slow rise of the intensity is associated with the latter stages (see Figure 5 and the values in Table 1).

Another parameter which provides information about the evolution of the system is the behavior of the stretching exponent obtained from the fits. This is depicted on a semilogarithmic scale in Figure 11. Although in stage 2 a power law fit is more appropriate, we plot in the figure the value of the exponent obtained from a stretched exponential fit. The stretched exponent α can give an indication of the width of distribution of decorrelation times at this stage and is used for comparison with the other stages. Similar to the decorrelation times, the exponent exhibits the same qualitative behavior at all temperatures. Initially, in stage 1, the values are scattered around 1 (depicted by the horizontal line). Then, at stage 2, α becomes lower than 1, in stage 3, α jumps to above 1, and finally, in stage 4 the exponent decreases again, below 1. Similar to what was obtained for the aging times, at higher temperatures the evolution of the exponent between the stages is faster (see Figure 11a). Therefore, if we plot the stretching exponents as a function of the normalized time defined above, we find correspondence between the different tendencies at the same effective ages. This is seen in Figure 11b and is similar to the behavior of the correlation times.

5. Discussion

The results of our SLS study of intensity variations following a temperature sweep are consistent with those of other investigators who used different experimental methods (calorimetry, rheology, etc.[36,38,39,41]) and concluded that there are two distinct gel states: at lower temperatures a "soft" gel is formed and at higher ones the system undergoes a transition into a "strong" gel state. In our experiment, the existence of the two gel states is manifested by the two-step increase of total scattered light intensity with temperature: a moderate one and a steep one corresponding to the soft and strong gel formation, respectively (see Figure 3). Measurements during very long aging times give us additional information about the evolution of the gel that has not been explored in previous studies. We find that the kinetics of gel formation is very slow and takes place over time scales of the order of days. The slow kinetics manifests itself in several ways. First, the strong hysteresis observed upon a temperature sweep (heating and cooling cycle) is an indication of slow processes that proceed at rates that are much smaller than the heating/cooling rates used. Furthermore, after long incubation times at elevated temperatures, gel dissolution upon decrease of the temperature shows even stronger hysteresis, due to the more robust network formed during the incubation. Another manifestation of the very slow kinetics is the very slow intensity increase at a constant temperature.

Gelation in MC gels is attributed to hydrophobic interaction between heavily methylated segments of the heteropolymer. Upon increasing the temperature, water becomes a poor solvent for MC (as this entropic interaction increases via the mechanism described in the Introduction) and the hydrophobic regions of different heterogeneously substituted polymers begin to aggregate leading to the formation of a macroscopic network. Since the hydrophobic segments of the chains are attached to the hydrophilic parts (which tend to be surrounded by water), full phase separation is suppressed. The aggregated hydrophobic domains serve as effective cross-links and a connected, gel-like structure results. Therefore, the gel can be described as a microphase separated system, different from a fully phase separated polymer−water solution. Further support for microphase separation as being the driving force for gelation is obtained by the peak of the scattered intensity at a finite q reported for the very similar cellulose analogue hydroxypropylcellulose,[65] which has many similarities to MC gels. In addition, the SANS behavior found by Lodge as a decrease with q^{-4} is typical of a two-phase system with sharp interfaces (Porod's scattering).[66] This Porod behavior at small length scales, which is progressively more pronounced with increase in time and temperature, reveals locally dense structures that grow as aggregation proceeds.

Our observations are consistent with the following model of the gel formation. The initial moderate increase of scattered intensity with temperature is caused by weak hydrophobic associations leading to the formation of a weakly cross-linked network ("weak gel"). The subsequent steep increase in the intensity at higher temperatures is due to increased strength of hydrophobic interactions that leads to gelation, with large hydrophobic aggregates acting as effective cross-links. Such aggregation processes create large polymer concentration gradients (and thus, large refractive index variations), resulting in enhanced light scattering in the "strong gel" phase.

In the strong gel domain, light scattering increases with both temperature and time. As the temperature is raised, the driving forces for phase separation become stronger resulting in increasingly larger and denser aggregates, and, consequently, to stronger light scattering. After reaching a steady temperature, the scattered intensity continues to increase with time but at progressively slower rates. From time scale decomposition of the intensity increase by CONTIN, we conclude that intensity stabilization occurs in two main stages. The first stage of rapid and strong increase in the intensity is the result of fast aggregation processes that lead to the initial buildup of the gel, at least on the length scale probed by our light scattering experiments. The second stage lasts days (its duration is longer at lower temperatures) and results in a relatively small increase in the scattered intensity. This stage corresponds to much slower rearrangements of the network as aggregates break and reassemble in order to increase the overlap between the hydrophobic groups and decrease the elastic energy of the stretched chains connecting the aggregates. After very long times (observed only at the highest temperature in our experiment) the scattered

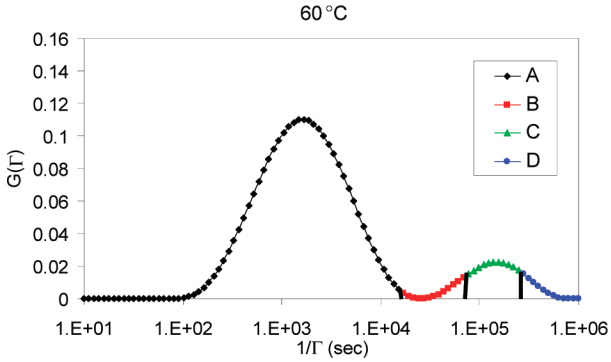

Figure 12. Decomposition of the scattered intensity increase at 60 °C of Figure 4 as shown in Figure 5 but with different stages in the evolution of the gel represented by different colors. Since the increase in the scattered intensity occurs upon heating and before temperature stabilization, a difference of ~7 min exists between the onsets of SLS and DLS measurements. This small shift is negligible on the time scales shown in the figure (notice the logarithmic scale on the horizontal axis).

intensity approaches a constant value indicating that the system approaches a macroscopic steady state.

DLS provides a closer view of the aging processes since it probes the microscopic dynamics of the system. We find that even after the scattered light intensity has almost stabilized, the speckle patterns continue to evolve with time and that the correlation between different speckle patterns taken at sufficiently well-separated times decays to zero, indicating that microscopic rearrangements, on length scales of the order of the probing wavelength, continue to take place in the gel. These rearrangements can be thought of as thermally induced "migration" of the gel through its configuration space, which is characterized by a broad distribution of local free energy minima. This picture is supported by the observation that shaking the gel raises the intensity of light scattered from it, presumably because shear reduces the free energy barriers for dissociation of chains from hydrophobic aggregates, thus enabling the system to move to a lower free energy state by increasing the number of hydrophobic contacts.

From measurements of the correlation functions at different aging times, we can identify four stages of aging, each of which is characterized by a different functional form of the decay of the correlations with time. Each stage has a different width of the distribution of relaxation times and this width changes in a characteristic way with aging time. Furthermore, the rate of increase of the decorrelation time with the aging time is different (see Figure 10) for the various stages. Finally, the rate of increase of total intensity during a stage is also different, as can be seen from comparison of the decorrelation times with the time scales of the increase of the scattered total intensity. This is shown in Figure 12 (for 60 °C as an example) and indicates that the first stage corresponds to the initial steep intensity rise, while the latter stages correspond to the more moderate subsequent increase of intensity.

On the basis of these experimental observations, we propose a tentative mechanism for the aging of the gel as the result of (a) the frozen in randomness of structure of MC polymers and (b) the interplay between hydrophobic interactions and elastic forces. During stage 1, the correlation function exhibits an almost exponential decay. Since the steep rise in the intensity with aging time occurs in this stage, we associate it with the formation and growth of aggregates. The gel begins to form through a sequence of nucleation events where small aggregates break and reform constantly (the hydrophobic interaction is of order of several kT per monomer), but those larger than some critical size continue to grow. The number of large aggregates

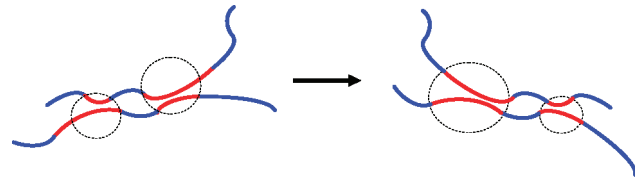

Figure 13. An example of an optimization process occurring during stage 2 where exchange of chains between two aggregates leads to greater overlap between hydrophobic segments. Blue curves denote hydrophilic segments and red curves denote the hydrophobic segments. Notice that the distribution of sizes of the aggregates becomes broader during this stage.

increases rapidly with time, leading to increased light scattering from the sample. Assuming that nucleation events are random and independent, the formation of hydrophobic aggregates can be described as a Poisson process, and since speckles appear as the result of interference of light scattered from such randomly distributed aggregates, one expects the correlation between speckle patterns to decay exponentially with time. This occurs along with *aggregate growth* as there are many hydrophobic segments still not linked and dissolved in the water. These chain portions may also reduce their energy by sticking onto the existing aggregates and thus increase the total scattered light intensity.

Stage 2 is characterized by a power law decay of the correlation function and a large increase of the decorrelation times with the aging time. Part of this stage corresponds to the first sharp intensity rise and extends until the scattered intensity rise begins to slow down. We associate this stage with an incubation period related to rearrangement of polymer chains in order to maximize the number of hydrophobic contacts inside the aggregates. An illustration of the sort of optimization process we believe take place is shown in Figure 13. While the size and number of clusters do not change significantly in this stage, their stability is strongly affected. The reason is that after the reorganization the bigger clusters have a much larger number of hydrophobic contacts (before, they were not optimized and thus could have a significant content of hydrophilic groups, because of chain connectivity). The result is that in stage 2 a broad distribution of cluster sizes (present already in stage 1) is translated into a broad distribution of relaxation times (lifetime increases with cluster size). Therefore, there is a large increase of time scales during this stage.

As aggregation proceeds, the hydrophilic chain segments connecting the aggregates formed by the hydrophobic segments are being progressively more stretched and elastic restoring forces set in. This partially arrests further separation and changes the relaxation behavior. The interplay between these two opposing forces is the cause for the slow microscopic rearrangements in MC gels in stages 3 and 4.

During the third stage the correlation function exhibits compressed exponential behavior. The time scales do not increase much and the total scattered intensity increase is small. We tentatively propose that elasticity starts to play a role in this stage, as the result of strong stretching of hydrophilic chain segments between aggregates formed in the previous stages. The broad distribution of stresses in the network is spatially nonuniform and local stresses may exceed a critical value for breakup of aggregates and nucleate fracture events. Such stress-induced processes may cause sudden and relatively abrupt events in parts of the network and result in faster than exponential dynamics occurring during this stage. We note that this does not contradict the persistent increase in the decorrelation time with aging as these elastic forces also cause the slowing down of aggregation processes. In addition, the driving force for further associations is strongly reduced in this stage since most hydrophobic segments are already linked. The resulting

process of large scale rearrangement of the network may be related to that observed in computer simulations of a simple model of phase separation of a chemical gels in poor solvent,[67] where fast avalanche-like processes leading to the formation of a network of high-density filaments were reported. Compressed exponential relaxation was also observed in a model[18] of nonpolymeric systems undergoing gelation, where processes contributing to the decorrelation were interpreted as "ballistic" motion resulting from relaxation of internal stresses in those systems.[67]

In stage 4 the exponent decreases again to a value below 1 and the time scales become significantly longer. We assume that at some point in the end of the rearrangement process of stage 3, the system finds a relatively stable configuration, or in other words, the system falls into one of the deep free energy minima from which the time to escape is relatively long. At this stage, the elastic stresses are balanced by the reduced driving forces for segregation resulting in sharply increased time scales and in the decrease of the exponent to below 1. The combined effects of growing relaxation times and increasingly stretched exponents cause the longest relaxation time in the system to exceed the laboratory time scale of observation in the system.

As already mentioned, although these processes take place at all temperatures, at higher temperatures the dynamics are faster due to the stronger driving forces for segregation which increases the rates of reorganization. Consequently, the transitions between stages are shifted to shorter aging times compared to those at lower temperatures.

Acknowledgment. We thank M. Gottlieb for providing the commercial MC samples, S. Greenstein for help with the experiments, and T. Lodge for sending us some of his raw data. Y.R. acknowledges the support of the Israel Science Foundation.

References and Notes

(1) See e.g.: Cipelletti, L.; Ramos, L. *Curr. Opin. Colloid Interface Sci.* **2002**, *7*, 228–234.
(2) Cates, M.; Evans, M. *Soft and fragile matter*; Institute of Physics Publishing: Bristol, UK, 2000.
(3) Henkel, M.; Pleimling M.; Sanctuary, R.; *Ageing and the Glass Transition*; Springer-Verlag: Berlin, 2005.
(4) Angell, C. A.; Ngai, K. L.; McKenna, G. B.; McMillan, P. F.; Martin, S. W. *J. Appl. Phys.* **2000**, *88*, 3113–3157.
(5) See e.g.: Binder, K.; Young, A. P. *Rev. Mod. Phys.* **1986**, *58*, 801–976.
(6) Fischer, K. H.; Hertz, J. A. *Spin Glasses*; Cambridge University Press: New York, 1991.
(7) Bouchaud, J. P.; Cugliandolo, L.; Kurchan, J.; Mezard, M. *Physica A* **1996**, *226*, 243–273.
(8) Gotze, W.; Sjorgen, L. *Rep. Prog. Phys.* **1992**, *55*, 241–376.
(9) Kob, W.; Barrat, J. *Phys. Rev. Lett.* **1997**, *78*, 4581–4584.
(10) Parisi, G. *Phys. Rev. Lett.* **1997**, *79*, 3660–3663.
(11) See e.g.: Cipelletti, L.; Ramos, L. *J. Phys.: Condens. Matter* **2005**, *17*, R253−R285, and references therein.
(12) Shibayama, M. *Bull. Chem. Soc. Jpn.* **2006**, *79*, 1799–1819.
(13) Cipelletti, L.; Bissig, H.; Trappe, V.; Ballesta, P.; Mazoyer, S. *J. Phys.: Condens. Matter* **2003**, *15*, S257−S262.
(14) Schupper, N.; Rabin, Y.; Rosenbluh, M. Manuscript in preparation.
(15) Cipelletti, L.; Manley, S.; Ball, R. C.; Weitz, D. A. *Phys. Rev. Lett.* **2000**, *84*, 2275–2278.
(16) Cipelletti, L.; Ramos, L.; Manley, S.; Pitard, E.; Weitz, D. A.; Pashkovski, E. E.; Johansson, M. *Faraday Discuss.* **2003**, *123*, 237–251.
(17) Ramos, L.; Cipelletti, L. *Phys. Rev. Lett.* **2001**, *87*, 245503.
(18) Bouchaud, J. P.; Pitard, E. *Eur. Phys. J. E* **2001**, *6*, 231–236.
(19) Klemm, D.; Philipp, B.; Heinze, T.; Heinze, U. Wagenknecht, W. *Comprehensive Cellulose Chemistry*; Wiley-VCH Verlag GmbH: Weinheim, FRG, 1998.
(20) Turak, A. F.; El-Kafrawy, A.; Snyder, F. W.; Auerbach, A. B. U.S. Patent 4,302,252, 1981.
(21) Isogai, A.; Ishizu, A.; Nakano, J. *Carbohydr. Res.* **1985**, *139*, 99–108.
(22) Isogai, A.; Ishizu, A.; Nakano, J. *J. Appl. Polym. Sci.* **1986**, *31*, 341–352.
(23) Petropavlovsky, G. A. *Hydrophilic partially substituted cellulose ethers and their modification by chemical cross-linking*; Nauka: Leningrad, 1988.
(24) Heymann, E. *Trans. Faraday Soc.* **1935**, *31*, 846–864.
(25) Takahashi, S.; Fujimoto, T.; Miyamoto, H.; Inagaki, H. *J. Polym. Sci., Part A, Polym. Chem.* **1987**, *25*, 987–994.
(26) Savage, A. *Ind. Eng. Chem.* **1957**, *49*, 99–103.
(27) Haque, A.; Morris, E. *Carbohydr. Polym.* **1993**, *22*, 161–173.
(28) Schupper, N.; Shnerb, N. M. *Phys. Rev. Lett.* **2004**, *93*, 037202.
(29) Schupper, N.; Shnerb, N. M. *Phys. Rev. E* **2005**, *72*, 046107.
(30) Rees, D. A. *Chem. Ind. (London)* **1972**, *19*, 630–636.
(31) Rees, D. A. *Adv. Carbohydr. Chem. Biochem.* **1969**, *24*, 267–332.
(32) Kato, T.; Yokoyama, M.; Takahashi, A. *Colloid Polym. Sci.* **1978**, *256*, 15–21.
(33) Tanford, C. *The Hydrophobic Effect, in Formation of Micelles and Biological Membranes*: John Wiley & Sons: New York, 1980.
(34) Sarkar, N. *J. Appl. Polym. Sci.* **1979**, *24*, 1073–1087.
(35) Kobayashi, K.; Huang, C.; Lodge, T. P. *Macromolecules* **1999**, *32*, 7070–7077.
(36) Li, L.; Thangamathesvaran, P. M.; Yue, C. Y.; Tam, K. C.; Hu, X.; Lam, Y. C. *Langmuir* **2001**, *17*, 8062–8068.
(37) Li, L.; Shan, H.; Yue, C. Y.; Lam, Y. C.; Tam, K. C.; Hu, X. *Langmuir* **2002**, *18*, 7291–7298.
(38) Desbrieres, J.; Hirrien, M.; Rinaudo, M. *Carbohydr. Polym.* **1996**, *31*, 243–252.
(39) Desbrieres, J.; Hirrien, M.; Ross-Murphy, S. B. *Polymer* **2000**, *41*, 2451–2461.
(40) Gaunet, J. M. *Thermoreversible gelation of polymers and biopolymers*; Academic Press: New York, 1992.
(41) Chevillard, C.; Axelos, M. A. V. *Colloid Polym. Sci.* **1997**, *275*, 537–545.
(42) Takahashi, M.; Shimazaki, M.; Yamamoto, J. *J. Polym. Sci., Part B, Polym. Phys.* **2001**, *39*, 91–100.
(43) Sarkar, N. *Carbohydr. Polym.* **1995**, *26*, 195–203.
(44) Schupper, N.; Rabin, Y.; Greenstein, S.; Rosenbluh, M. *Opt. Eng.* **2004**, *43*, 398–406.
(45) Dainty, J. C. *Laser Speckle and Related Phenomena*, Springer-Verlag: Berlin, 1984.
(46) Wong, A. P. Y.; Wiltzius, P. *Rev. Sci. Instrum.* **1993**, *64*, 2547–2549.
(47) Kirsch, S.; Frenz, V.; Schartl, W.; Bartsch, E.; Sillescu, H. *J. Chem. Phys.* **1996**, *104*, 1758–1761.
(48) Bartsch, E.; Frenz, V.; Kirsch, S.; Schartl, W.; Sillescu, H. *Prog. Colloid Polym. Sci.* **1997**, *104*, 40–48.
(49) Cipelletti, L.; Weitz, D. A. *Rev. Sci. Instrum.* **1999**, *70*, 3214–3221.
(50) Freund, I. *Physica A* **1990**, *168*, 49–65.
(51) Berne, B. J.; Pecora, R. *Dynamic Light Scattering*; John Wiley & Sons: New York, 1976.
(52) Desbrieres, J.; Hirrien, M.; Rinaudo, M. *Carbohydr. Polym.* **1998**, *37*, 145–152.
(53) CONTIN Matlab program, Supplied by Magritek .
(54) Boyko, V.; Richter, S. *Macromol. Chem. Phys.* **2004**, *205*, 724–730.
(55) Ren, S. Z.; Sorensen, C. M. *Phys. Rev. Lett.* **1993**, *70*, 1727–1730.
(56) Okamoto, M.; Norisuye, T.; Shibayama, M. *Macromolecules* **2001**, *34*, 8496–8502.
(57) Ikkai, F.; Shibayama, M. *Phys. Rev. Lett.* **1999**, *82*, 4946–4949.
(58) Bellour, M.; Knaebel, A.; Harden, J. L.; Lequeux, F.; Munch, J.-P. *Phys. Rev. E* **2003**, *67*, 031405.
(59) Abou, B.; Bonn, D.; Meunier, J. *Phys. Rev. E* **2001**, *64*, 021510.
(60) Bouchaud, J. P.; Cugliandolo, L. F.; Kurchan, J.; Mezard, M. In *Spin Glasses and Random Fields*; Young, A. P., Ed.; World Scientific: Singapore:, 1998.
(61) Knaebel, A.; Bellour, M.; Munch, J. P.; Viasnoff, V.; Lequeux, F.; Harden, J. L. *Europhys. Lett.* **2000**, *52*, 73–79.
(62) Bissig, H.; Romer, S.; Cipelletti, L.; Trappe, C.; Schurtenberger, P. *PhysChemComm.* **2003**, *6*, 21–23.
(63) El Masri, D.; Pierno, M.; Berthier, L.; Cipelletti, L. *J. Phys: Condens. Matter* **2005**, *17*, S3543−S3549.
(64) Kita, R.; Kaku, T.; Kubota, K.; Dobashi, T. *Phys. Lett. A* **1999**, *259*, 302–307.
(65) Porod, G. *Kolloid Z.* **1951**, *124*, 83–111.
(66) Peleg, O.; Kroger, M.; Hecht, I.; Rabin, Y. *Europhys. Lett.* **2007**, *77*, 58007–58011.
(67) The existence of opposing forces in the system is the source of the difference between MC and other, nonpolymeric, physical gels. In the former, chain connectivity plays an important role in the late stages of the aging process, while in colloidal gels the constituents are not interconnected and dynamics is driven by attractive or repulsive interactions only. As a consequence, the form of the correlation function for nonpolymeric physical gels does not change with aging time.

MA702613J